

FULL PAPER

Open Access



Coseismic deformation due to the 2011 Tohoku-oki earthquake: influence of 3-D elastic structure around Japan

Akinori Hashima^{1*} , Thorsten W. Becker^{2,3}, Andrew M. Freed⁴, Hiroshi Sato¹ and David A. Okaya²

Abstract:

We investigated the effects of elastic heterogeneity on coseismic deformation associated with the 2011 Tohoku-oki earthquake, Japan, using a 3-D finite element model, incorporating the geometry of regional plate boundaries. Using a forward approach, we computed displacement fields for different elastic models with a given slip distribution. Three main structural models are considered to separate the effects of different kinds of heterogeneity: a homogeneous model, a two-layered model with crust–mantle stratification, and a crust–mantle layered model with a strong subducting slab. We observed two counteracting effects: (1) On large spatial scales, elastic layering with increasing rigidity with depth leads to a decrease in surface displacement. (2) An increase in rigidity from above the slab interface to below causes an increase in surface displacement, because the weaker hanging wall deforms to accommodate coseismic slip. Results for slip inversions associated with the Tohoku-oki earthquake show that slip patterns are modified when comparing homogeneous and heterogeneous models. However, the maximum slip only changes slightly: It increases from 38.5 m in the homogeneous to 39.6 m in the layered case and decreases to 37.3 m when slabs are introduced. Potency, i.e., the product of slip and fault area, changes accordingly. Layering leads to inferred slip distributions that are broader and deeper compared to the homogeneous case, particularly to the south of the overall slip maximum. The introduction of a strong slab leads to a reduction in slip around the slip maximum near the trench. We also find that details of the vertical deformation patterns for heterogeneous models are sensitive to the Poisson's ratio. While elastic heterogeneity does therefore not have a dramatic effect on bulk quantities such as inferred potency, the mechanical response of a layered medium with a slab does lead to a systematically modified slip response, and such effects may bias studies of mega-thrust earthquakes.

Keywords: 2011 Tohoku-oki earthquake, Elastic structure, Finite element model, Slip inversion, GPS observation

Introduction

The 2011 M9 Tohoku-oki earthquake, Japan, is one of the largest earthquakes ever observed, causing an abrupt change in regional seismicity and large-scale crustal deformation (e.g., Nishimura et al. 2011; Ishibe et al. 2011; Fig. 1). Given the mandate of improving our understanding of the associated seismic hazard, and utilizing the well-instrumented deformation signatures of this earthquake for our understanding of crustal mechanics,

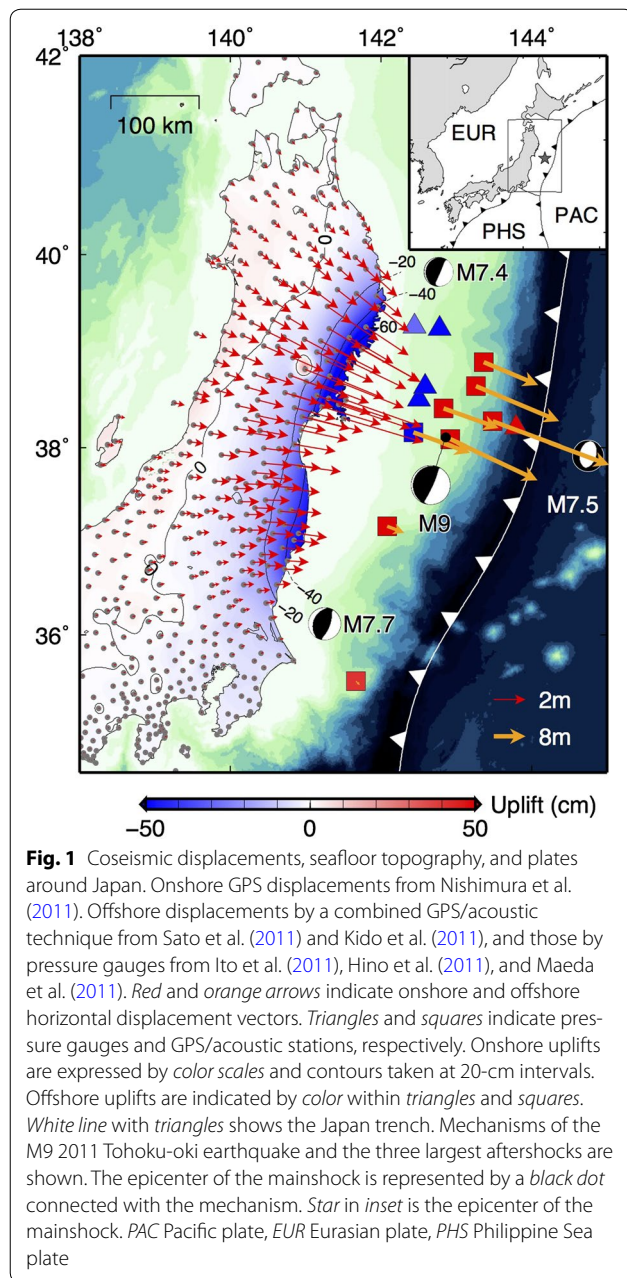
it is important to understand the coseismic slip, and how it may be influenced by the heterogeneity of the elastic structure that surrounds the plate interface.

The coseismic slip of the Tohoku-oki earthquake has been estimated from various observations including teleseismic waveforms (e.g., Yagi and Fukahata 2011), strong motion (e.g., Suzuki et al. 2011), and tsunami propagation (e.g., Fujii et al. 2011), as well as from geodesy. The Japanese islands are covered with one of the world's most dense GPS networks and seafloor geodetic stations that recorded coseismic surface displacements caused by the earthquake (Fig. 1). A number of geodetic slip inversions have been published, most of which used response (Green's) functions computed with the assumption of a

*Correspondence: hashima@eri.u-tokyo.ac.jp

¹ Earthquake Research Institute, University of Tokyo, Yayoi 1-1-1, Bunkyo-ku, Tokyo 113-0032, Japan

Full list of author information is available at the end of the article



homogeneous elastic half-space (e.g., Ozawa et al. 2011, 2012; Iinuma et al. 2011, 2012; Perfettini and Avouac 2014), which is often an adequate approximation. However, the great spatial extent of the Tohoku-oki earthquake, more than 500 km along the surface, causing stress changes to similar depth extent, makes it likely that the resulting surface deformation was affected by the heterogeneity of the surrounding structure. Those include lateral variations in elastic strength due to the presence of the slab as well as depth dependence due to the influence of pressure and temperature on elastic strength.

For example, the consideration of elastic moduli increasing with depth may lead to an increase in inferred seismic moment compared to a homogeneous model (e.g., Hearn and Bürgmann 2005; Pollitz et al. 2011; Diao et al. 2012; Dong et al. 2014). Conversely, the consideration of a strong slab (a slab with increased rigidity) in the coseismic inversion was shown to lead to a decrease in inferred seismic moment compared to a homogeneous model (Hsu et al. 2011; Kyriakopoulos et al. 2013). Consideration of surface topography and lateral heterogeneity from seismic tomography was also found to lead to a better fit to the observed coseismic surface displacements (Pulvirenti et al. 2014; Romano et al. 2014). There is, however, significant uncertainty when seismic velocity is converted to elastic moduli because of the possibly competing effects of temperature, pressure, and composition. Moreover, the physical mechanisms as to how different kinds of elastic heterogeneity affect surface deformation are unclear.

Here, we develop a 3-D finite element model that systematically investigates the kinematics of the Tohoku-oki earthquake given different structural configurations in order to understand how the various components influence the inferred slip distribution and seismic moment. This complexity includes depth-dependent elastic structure (including a Moho interface), as well as the incorporation of both the Pacific (PAC) and Philippine Sea Plate (PHS) slabs. We also study what level of complexity may be required to accurately explain both horizontal and vertical onland GPS, as well as seafloor geodetic observations.

Methods

We model elastic structure corresponding to crust–mantle layering under northeast Japan on the Eurasian plate (EUR) and the descending PAC and PHS slabs with a finite element method. Effects of elastic structure on coseismic deformation are evaluated by the following steps: (1) compute deformation due to a slip distribution given by a simple model to resemble the actual slip distribution of the Tohoku-oki earthquake for different structures (forward test) in order to get an understanding of the characteristic patterns and (2) invert for the actual slip distributions based on the data using Green's functions for slip patches computed for different elastic structures.

Finite element modeling

We use the ABAQUS finite element modeling software (<http://www.3ds.com>) to model coseismic deformation. To minimize boundary effects, our model domain includes the regions surrounding the immediate study area: the Kuril arc to the northeast, the Izu–Bonin

and Mariana arcs to the south, and the Ryukyu arc to the southwest (Fig. 2). The model domain is taken as a $3700 \text{ km} \times 4600 \text{ km}$ rectangular region with a depth of 700 km. Geometric features expressed in spherical coordinates are transformed into Cartesian using an azimuthal equidistant projection taking (140°E , 40°N) as the center point. Displacements on the lateral and bottom boundaries of the model domain are fixed to zero. We have verified that the boundaries are far enough from the study area so as not to influence the model results.

The geometry of the PAC–EUR/PHS and PHS–EUR plate boundaries is estimated from interplate seismicity. We follow Nakajima and Hasegawa (2006), Nakajima et al. (2009), and Kita et al. (2010) for the PAC–EUR/PHS boundary under northeast Japan, and Baba et al. (2002), Nakajima and Hasegawa (2007), Hirose et al. (2008a, b), and Nakajima et al. (2009) for the PHS–EUR boundary under southwest Japan. The PAC–EUR plate boundary under the Kuril arc, the PAC–PHS boundary under the Izu–Bonin and Mariana arcs, and the PHS–EUR boundary under the Ryukyu arc are summarized in the Slab1.0 model (Hayes et al. 2012). We interpolate these models to smooth PAC–EUR/PHS and PHS–EUR plate boundaries with the method of minimizing curvature with tension (Smith and Wessel 1990) and implement them into the finite element model. The plate boundaries divide the model domain into EUR, PAC, and PHS parts (Fig. 2a). The top of EUR is taken as a flat surface at $z = 0 \text{ km}$ and the top of PAC and PHS is taken flat at $z = -5 \text{ km}$, considering the relative elevation of continents and oceans. We also implement interfaces representing the lower surface of the subducting PAC and PHS plates. Slab thickness is assumed to be 70 km based on seismicity and seismic tomography (e.g., Nakajima and Hasegawa 2006). The crust–mantle boundary for EUR is set at $z = -30 \text{ km}$, which is the average value around Japan (e.g., Matsubara et al. 2008). Each part is subdivided into a number of layers as shown in Fig. 2c, d, which allows to set vertical variation in elastic moduli within the part. We do not consider minor surface topographic features nor anomalies in the Moho depth and slab thickness in our model, for simplicity. The model domain is divided into $\sim 1,000,000$ linear, tetrahedral elements. The characteristic length of the elements is $\sim 5 \text{ km}$ near the fault region and $\sim 100 \text{ km}$ on the lateral side and bottom of the model domain (Fig. 2a). We have verified that further refinement of the mesh led only to minor changes in the predicted displacement field.

The fault slip region is assumed to be the PAC–EUR, PHS–EUR, and PAC–PHS plate boundaries shallower than 80 km depth, which are divided into 32×8 , 17×8 , and 11×8 subfaults (or patches) of uniform slip, respectively (Fig. 2b). Slip on a subfault is prescribed using

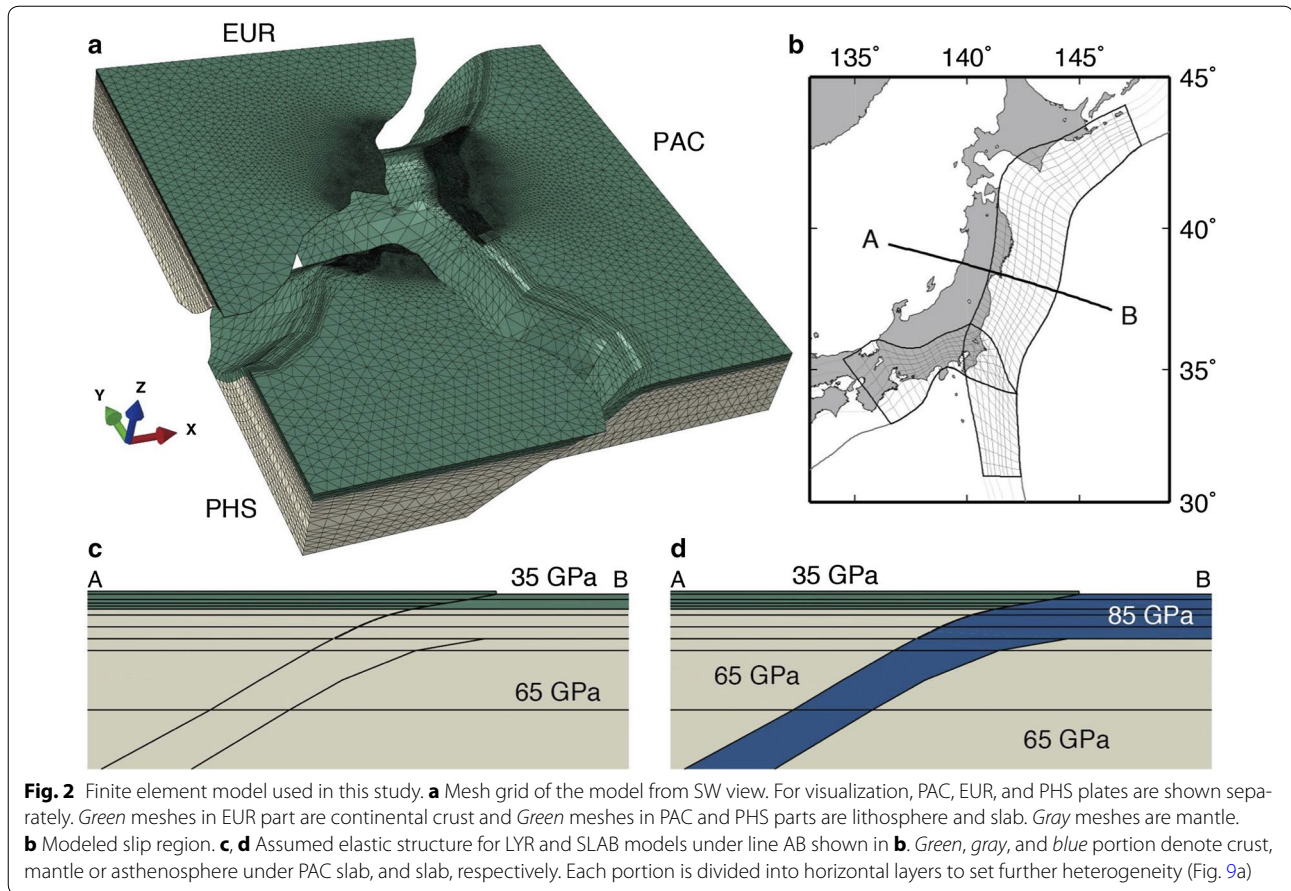
constraint equations defining relative movement of the two surfaces separated by a small distance (no contact condition), allowing the computation of Green's functions.

In terms of elastic heterogeneity, we consider the effects of crust–mantle layering and strong slabs (Fig. 2d). Three structures are considered: (1) a homogeneous model (HOM), (2) a two-layered model with the layer interface at $z = -30 \text{ km}$ (LYR) (Fig. 2c), and (3) a two-layered in the EUR part with added PAC- and PHS-slab model (SLAB) (Fig. 2d). The rigidity for HOM is assumed to be 35 GPa (deformation for homogeneous model is independent of rigidity). Considering seismic velocity structure beneath Japan and V_p - and V_s -anomalies of the slab for guidance (e.g., Nakajima et al. 2001; Matsubara et al. 2008; Huang et al. 2011), values for the rigidity of the crust, mantle, and slab in LYR and SLAB are set to 35, 65, and 85 GPa, respectively, and the Poisson's ratio is set to 0.25 for all materials. Note that average rigidity for the model increases in order of HOM, LYR, and SLAB. For each elastic structure, displacement responses of the onshore and offshore stations for unity strike and dip slips on all subfaults are calculated as Green's functions for inversion of the observed data.

Observed coseismic displacements

The Japanese islands are covered by a network with more than 1200 permanent GPS stations run by the Geospatial Information Authority (GSI) of Japan (e.g., Sagiya et al. 2000). GSI releases daily site location solutions of the stations estimated by routine analysis. However, daily locations include the effect of plenty of aftershocks for Tohoku-oki, including the three M7 aftershocks that occurred within 30 min after the M9 mainshock. Nishimura et al. (2011) estimated 5-min locations by kinematic positioning analysis to remove aftershock effects. We used 1283 data from Nishimura et al. (2011). Observational errors of GPS measurements on land are ~ 4 and $\sim 15 \text{ mm}$ for horizontal and vertical components, respectively (e.g., Ozawa et al. 2011).

In addition to the onshore data, we can use the data at six Japan Coast Guard and two Tohoku University seafloor stations, obtained by a combined GPS/acoustic technique (Sato et al. 2011; Kido et al. 2011). We also use vertical displacement data obtained by four pressure gauge results of Tohoku University (Ito et al. 2011; Hino et al. 2011) and two from the Earthquake Research Institute of the University of Tokyo (Maeda et al. 2011). A station of Tohoku University named GJT3 observes vertical displacements with both a GPS/acoustic technique and a pressure gauge. As the pressure gauge data are considered to be of higher accuracy (Iinuma et al. 2012), we use pressure gauge data as the vertical displacement for



GJT3. The observational errors are of order hundred millimeters (Sato et al. 2011), i.e., much larger than those of onshore data. The offshore data are also contaminated by the effect of foreshocks and aftershocks. However, these effects are estimated to be relatively small, and so the seafloor data give us important information complementing onshore data (Sato et al. 2011).

Figure 1 shows both onshore and offshore data. We can see broad horizontal deformation of ~ 5 m at the maximum on land and ~ 31 m on the seafloor. On the other hand, vertical deformation is relatively localized on the Pacific coast with maximum 1.1 m subsidence on land and 5 m uplift on the seafloor.

Inversion

We perform a standard, damped linear inversion (e.g., Menke 2012). Considering linear elasticity, the displacement data \mathbf{d} and slip \mathbf{x} can be related to the response matrix \mathbf{A} as,

$$\mathbf{d} = \mathbf{A}\mathbf{x}. \quad (1)$$

Here, \mathbf{d} and \mathbf{A} are scaled by the data uncertainties. We require a smooth slip distribution, whose roughness may be expressed by using the Laplace operator as

$$\mathbf{L} = \sum_{i=1}^2 \int_S \left(\frac{\partial^2 x^i}{\partial \xi_1^2} + \frac{\partial^2 x^i}{\partial \xi_2^2} \right)^2 d\xi_1 d\xi_2 \quad (2)$$

where ξ_1 and ξ_2 are local coordinates along strike and dip direction. Superscript i is taken for strike and dip components. Discretizing Eq. (2), we can obtain the vector form of the smoothness constraints,

$$\alpha \mathbf{L}\mathbf{x} = 0. \quad (3)$$

Here, \mathbf{L} is the roughness matrix, i.e., a discretized Laplace operator, and α is a damping parameter. Because there are places where arrangement of the subfaults is highly oblique, explicit expressions for \mathbf{L} can become involved as shown in “Appendix” section. The slip vector \mathbf{x} is obtained by solving Eqs. (1) and (3) by damped least squares

$$\mathbf{x}_{BF} = \left(\mathbf{A}^T \mathbf{A} + \alpha^2 \mathbf{L}^T \mathbf{L} \right)^{-1} \mathbf{A}^T \mathbf{d}. \quad (4)$$

In order to determine α , we compute a trade-off curve by plotting variance reduction defined as $(1 - (\mathbf{d} - \mathbf{A}\mathbf{x})^T (\mathbf{d} - \mathbf{A}\mathbf{x})) / (\mathbf{d}^T \mathbf{d})$ and roughness $(\mathbf{L}\mathbf{x})^T \mathbf{L}\mathbf{x}$ for variable values of α . A preferred solution satisfying

both data fit and smoothness of solution may be obtained at a shoulder point of the trade-off curve (Fig. 3). The covariance matrix of the solution parameters is given by

$$[\text{cov } \mathbf{x}] = \left(\mathbf{A}^T \mathbf{A} + \alpha^2 \mathbf{L}^T \mathbf{L} \right)^{-1}. \quad (5)$$

It would be difficult to reproduce the seafloor displacements if we would assign data uncertainties based on observation errors in the inversion, because of asymmetries of numbers of the onland GPS data and the numbers of the seafloor data and because of the difference in observation errors of the seafloor stations. As Iinuma et al. (2012) pointed out, the model error of the response matrix due to spatial heterogeneity might be up to 10 % of the amplitude of the data. In this study, we assume an additional weight for seafloor data. We use weights of 1:¼:1/10 for horizontal components of the onshore data, vertical components of the onshore data, and seafloor displacements, respectively. The effect of this weighting is explored below.

Results

Forward tests

Based on previous studies that inferred largest slip values near the trench (e.g., Ozawa et al. 2012), a simple slip distribution for the forward tests is assigned to the sub-faults in a concentric fashion with the center of (144°E, 37.8°N) (Fig. 4). The slip direction is parallel to line *ab* in Fig. 4, and slip decreases linearly from 40 m at the

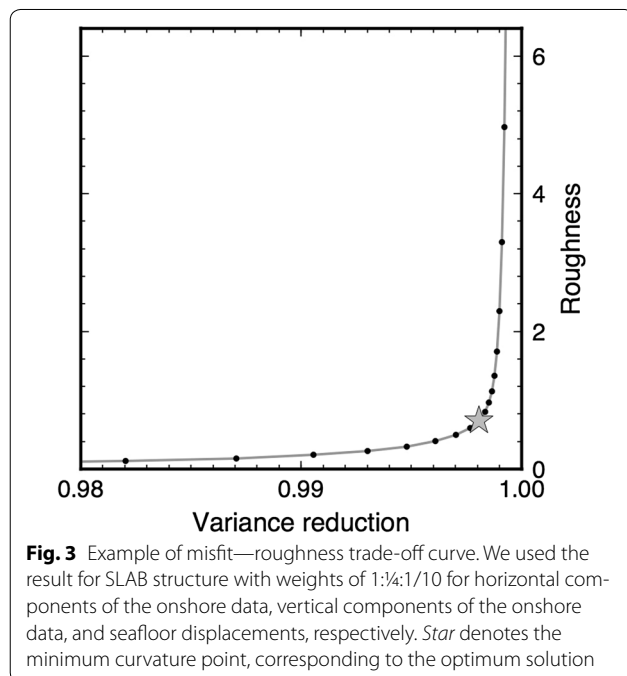
center to zero at the distance of 200 km. The equivalent seismic moments are 5.01×10^{22} Nm, 5.82×10^{22} Nm, and 9×10^{22} Nm for the HOM, LYR, and SLAB cases, respectively. These differences arise from differences in rigidity. The potency, i.e., the product of slip and fault area alone, is identical for all cases, at 1.43×10^{12} m³.

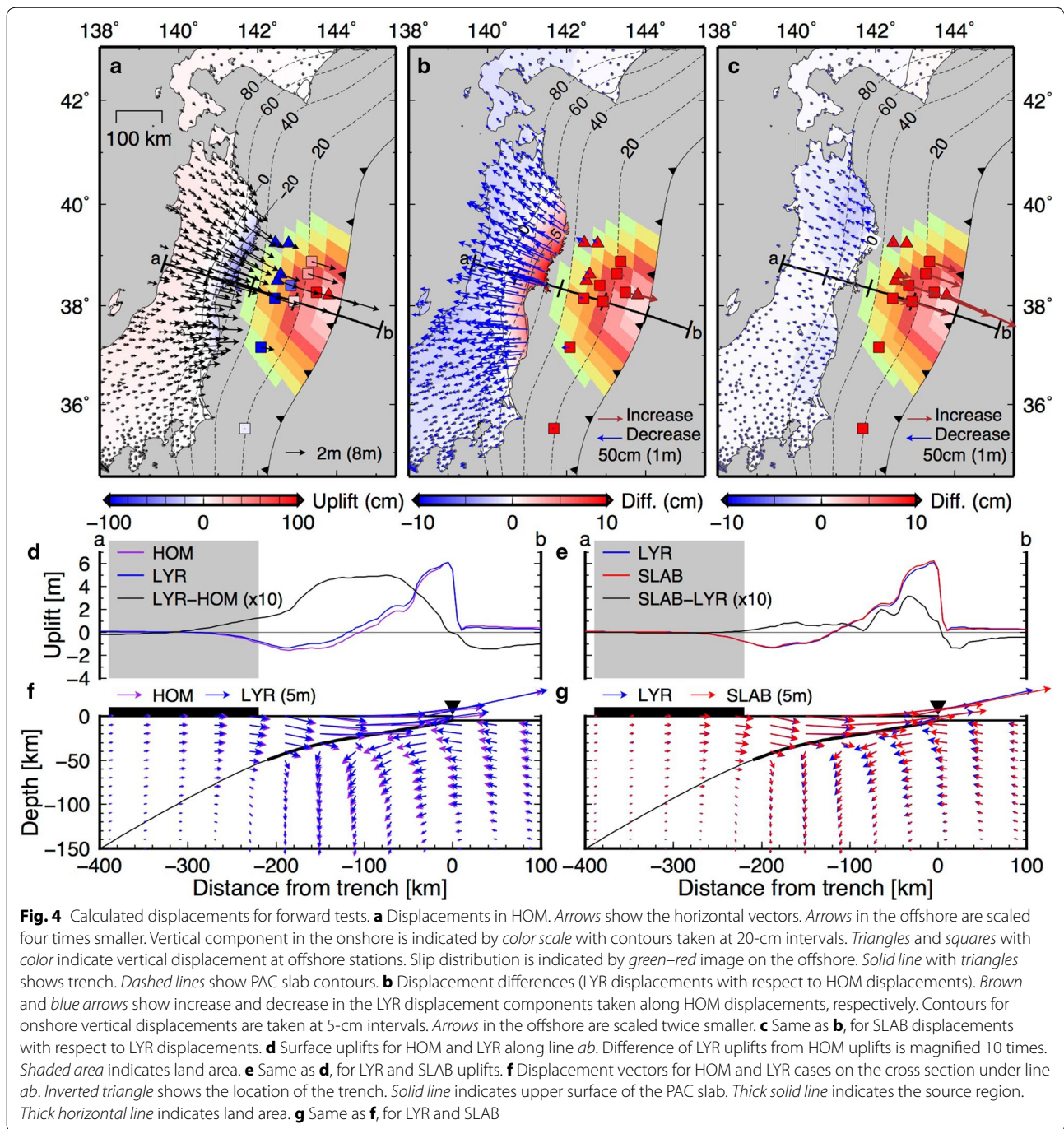
Figure 4a shows the surface displacement field for the HOM case, but visually results are very similar for all structures: Horizontal displacement vectors point toward the source region with a maximum magnitude of ~5 m onshore and ~20 m offshore. Vertical displacements show uplifts up to 5 m near the trench, subsidence at distances of 100–300 km from the trench, and gentle uplift further away. We can see the subtle effects of crust–mantle layering by subtracting HOM displacements from LYR displacements and those of the strong slab by subtracting LYR from SLAB displacements. We plot differences in displacements at the observation stations, surface vertical displacements along line *ab*, and displacement fields on a cross section with depth under line *ab* for LYR–HOM (Fig. 4b, d, f) and for SLAB–LYR (Fig. 4c, e, g).

The crust–mantle layering leads to a decrease in magnitude of the onshore horizontal vectors of LYR compared to HOM (Fig. 4b). At the same time, a comparable amount of increase at stations near the trench is inferred. As for vertical displacements, relative uplift up to ~300 km from the trench, and relative subsidence further than ~300 km away from the trench are found (Fig. 4b, d). Figure 4f shows an overall decrease in the magnitude of the displacement vectors both in the hanging wall and in the footwall except above the shallow part of the source region. The less deformable mantle impedes the relative displacement motions.

In the case of the SLAB–LYR difference, displacement differences are expectedly more localized around the source region near the trench because of the introduction of the strong slab. However, Fig. 4c also shows an onshore decrease and offshore increase in magnitude of the horizontal vectors of SLAB compared to LYR. In this case, the offshore difference is more than ten times larger. The vertical difference shows offshore relative uplift and onshore relative subsidence. Interestingly, the surface vertical difference appears to have two individual uplift zones at ~0–100 and ~100–300 km from the trench along line *ab* (Fig. 4e). The displacement difference is larger to the north of the line *ab* (Fig. 4c), due to the proximity of the land area to the source region and asymmetry in geometry of the plate interface.

Thus, crust–mantle layering and slab effects can show contrasting behaviors of increases in offshore displacement and decreases onshore, though the pattern and relative amplitude differ. We can understand these effects as a superposition of two contributions. The first, *layering*





effect is an overall decrease in deformation with increase in average rigidity across the model region. The second, *interface* effect is local to the source/trench region: When the rigidity of the footwall is relatively larger than the hanging wall, the footwall becomes less deformable. Thus, for the same slip, the movement of the hanging wall should increase (cf. Hsu et al. 2011). Both effects exist in

the HOM → LYR and LYR → SLAB steps. In LYR, material just above and beneath the plate interface is the same, but the underlying high rigidity layer results in less deformation in the footwall side, causing an interface effect. In SLAB, an increase in rigidity from LYR occurs only in the thin slab zone, but still contributes to the increase in average rigidity. Thus, we can see the layering effect on

land, though it is very small. The contrasting behavior thus appears as the superposition of the two effects in both steps.

We can expect the two effects to be seen in vertical displacements as well. Though vertical displacements are harder to explain because of the inverse of the sign from offshore to onshore, the two effects can account for an increase in uplift near the trench and slight decrease in uplift on the west coast. On the other hand, relative uplift occurs ~ 100 – 300 km from the trench including several seafloor stations near the land and coastal areas, where the two effects cancel for the horizontal case (Fig. 4d, e). This uplift zone is distinguishable from the uplift zone at ~ 0 – 100 km from the trench in Fig. 4e. Figure 4f, g shows a decrease in descending motion of the footwall beneath the relative uplift area (at ~ 100 – 200 km from the trench). Hence, this relative uplift may be the result of blocking of the descending motion due to the high rigidity of the mantle and slab.

In Fig. 5, we show how these elastic effects depend on the choice of the structural parameters: mantle rigidity μ_m in LYR, slab rigidity μ_s in SLAB, crustal thickness H in LYR, and the Poisson's ratio, ν , of the continental crust in SLAB. Both horizontal and vertical profiles are shown along line *ab*.

The layering and interface effects expectedly increase with an increase in the rigidity contrast. The displacement difference changes in magnitude, while the pattern remains the same (Fig. 5a–d). Changes in crustal thickness lead to more complex results. In the horizontal profile, heterogeneous effects become less pronounced when the thickness both increases and decreases from LYR model ($H = 30$ km) (Fig. 5c). In the limit of both $H \rightarrow 0$ and $H \rightarrow \infty$, LYR model becomes the homogeneous model. The layering effect reaches its maximum when the crustal thickness is equal to the vertical extent of the source region (~ 35 km). On the other hand, the layering effect in the verticals is not reduced for $H = 60$ or 80 km (Fig. 5d). We can see that a significant LYR–HOM difference in downward displacement occurs at depths of ~ 100 km (Fig. 4f), so layering down to this depth may still influence surface vertical displacements. Changing the Poisson's ratio for the continental crust does not lead to large changes in the horizontals, but strongly affects verticals in response to horizontal extension (Fig. 5g, h), even leading to change in the sign of the difference of the vertical fields for the SLAB versus the LYR case. Hence, high Poisson's ratios could lead to an underestimate of vertical displacements.

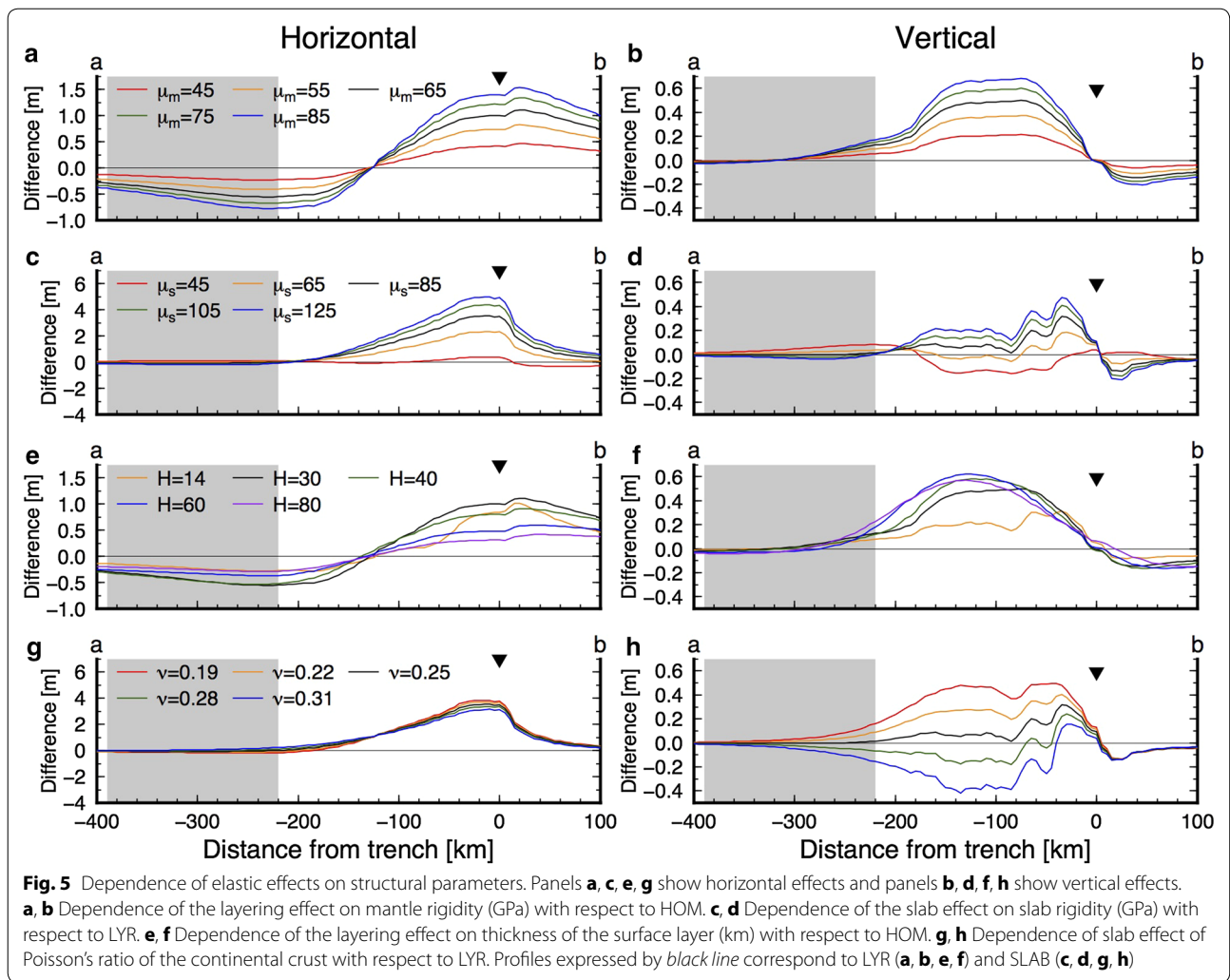
Slip inversion

Figure 6a shows the best-fitting solution for the SLAB case, and Fig. 6b shows the uncertainty in slip obtained

by taking the square root of the diagonal elements of the covariance matrix (Eq. 5). We also estimated uncertainties by Monte Carlo simulations, assigning normally distributed random perturbations to the data and then inverting 5000 realizations of those synthetics; the mean solution is the same as Fig. 6a and the resulting error (standard deviation) shown in Fig. 6c. We consider the Monte Carlo estimates of slip uncertainties (Fig. 6c), which are \sim one-third of the amplitude of the analytical estimates (Fig. 6b), to be closer to the true uncertainty, but in Fig. 6b errors are more conservative. Next, we examined the contribution of slip on the PHS slab by comparing inversions with and without the PHS source region (Fig. 6d). The comparison shows that the effect of allowing slip on the PHS interface is minor. While the modifications in the overall slip pattern seem physically plausible, at least close to the southern trench, their amplitude is less than, or comparable to, what one would expect from the conservative or Monte Carlo-based “noise” estimates, respectively. In the following, we will allow for slip on the PHS interface, but note that overall results do not critically depend on this choice.

Results for slip inversions with the different elastic structures are shown in Fig. 7. Upper panels (Fig. 7a–c) show results using both onshore and offshore data, and lower panels (Fig. 7d–f) for results using only onshore data. Figure 7a, d shows inversion results for HOM. Figure 7b, e shows slip vectors of LYR subtracting HOM slip, and Fig. 7c, f shows SLAB subtracting LYR. Calculated surface displacements are shown in Fig. 8. Upper panels show results using both onshore and offshore data, and lower panels for results using only onshore data. Figure 8a, e shows comparison of the calculated and observed displacements for HOM. Figure 8b, f shows residual (observed minus computed) displacements for HOM, Fig. 8c, g for LYR, and Fig. 8d, h for SLAB. Parameters for slip distribution and data fitting in each case are summarized in Table 1.

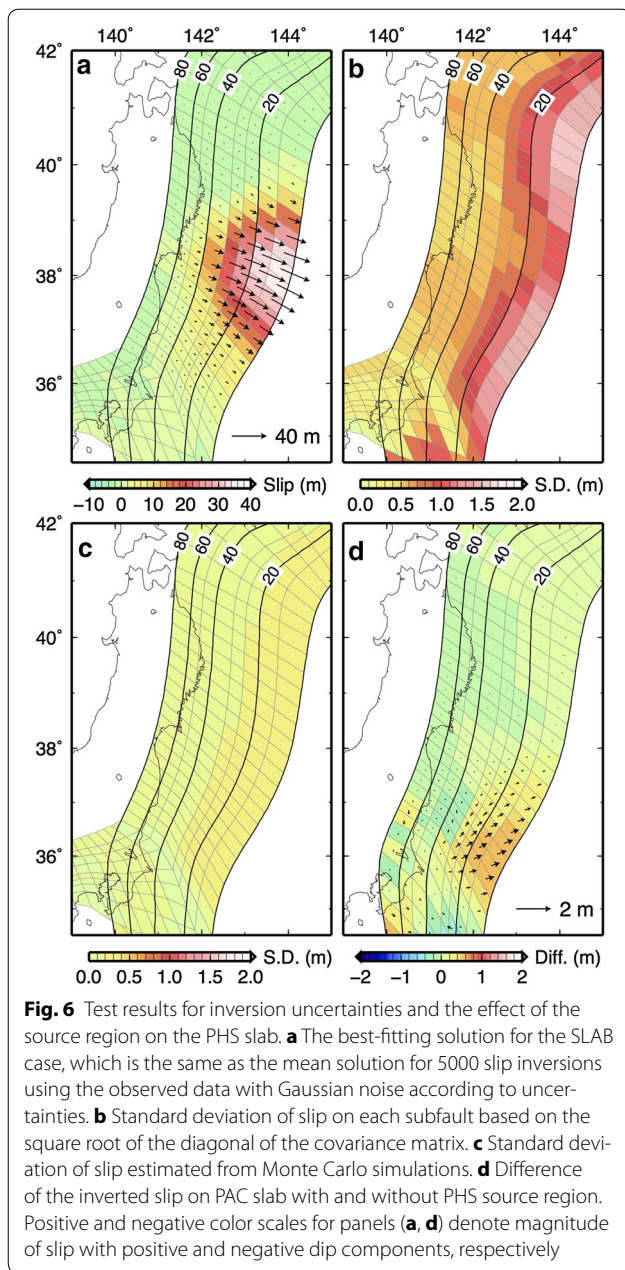
As expected from the forward tests, the basic slip pattern for HOM (Fig. 7a) is common to each structure. The maximum slip of 38.5 m occurs near the trench at 38°N with corresponding seismic moment of 3.72×10^{22} Nm. These values are consistent with previous estimates assuming a homogeneous structure, though published maximum slip values vary widely, from ~ 30 to ~ 80 m, depending on the choice of data weights and smoothing constraints (e.g., Pollitz et al. 2011; Diao et al. 2012; Iinuma et al. 2012; Ozawa et al. 2012; Perfettini and Avouac 2014). In the LYR case, the slip area broadens as indicated by the slip difference (Fig. 7b). The maximum slip increases to 39.6 m, but a larger, local increase of ~ 3 m occurs at 37°N . Seismic moment increases to 4.49×10^{22} Nm, corresponding to the moment



magnitude of 9.04. In the SLAB case, the maximum slip drops to 37.3 m, while the seismic moment and the moment magnitude further increase to 7.16×10^{22} Nm and 9.17, respectively. We can see a local slip increase area at 40°N (Fig. 7c). This increase appears to cancel out the negative dip slip seen for HOM (Figs. 6a, 7a). The increase in seismic moment from HOM, to LYR, to SLAB mostly reflects the increase in rigidity in the surrounding material. Potency is more appropriate for comparisons of slip characteristics (e.g., Ampuero and Dahlen 2005; Hearn and Bürgmann 2005) and increases from 1.06×10^{12} m³ (HOM) to 1.18×10^{12} m³ (LYR) and then drops slightly to 1.16×10^{12} m³ (SLAB) as does the maximum slip (Table 1). The residual displacements (Fig. 8b–d) decrease in both horizontal and vertical components, and at both onshore and offshore stations, indicating an improvement of fit using SLAB or LYR compared to the HOM case. Looking at the residuals in detail, the decrease in residual occurs more to the south at $37\text{--}38^\circ\text{N}$

at the HOM \rightarrow LYR step (Fig. 8b, c), and the remaining residual at $\sim 40^\circ\text{N}$ diminishes for the LYR \rightarrow SLAB step (Fig. 8c, d). These changes appear related to the movement of the area of slip change from $\sim 37^\circ\text{N}$ (Fig. 7b) to $\sim 38^\circ\text{N}$ (Fig. 7c). In terms of variance reduction, the layering effect is dominant in improving the HOM model, but the slab also contributes to an improvement (Table 1).

Results for the onshore only inversion show similar features to those for the full inversion. Compared to the results for the combined inversion, the slip in HOM is more broadly distributed, and the maximum slip decreases to 22.4 m, which is consistent with other studies without offshore data (Ozawa et al. 2011; Iinuma et al. 2011). The maximum slip slightly increases to 23.2 m in LYR and then decreases to 22 m in SLAB model. Potency shows a similar trend, from 0.95×10^{12} m³ (HOM) to 1×10^{12} m³ (LYR) and 0.97×10^{12} m³ (SLAB). The seismic moment increases steadily from 3.31×10^{22} Nm (HOM), through 4.01×10^{22} Nm (LYR), to 6.07×10^{22} Nm



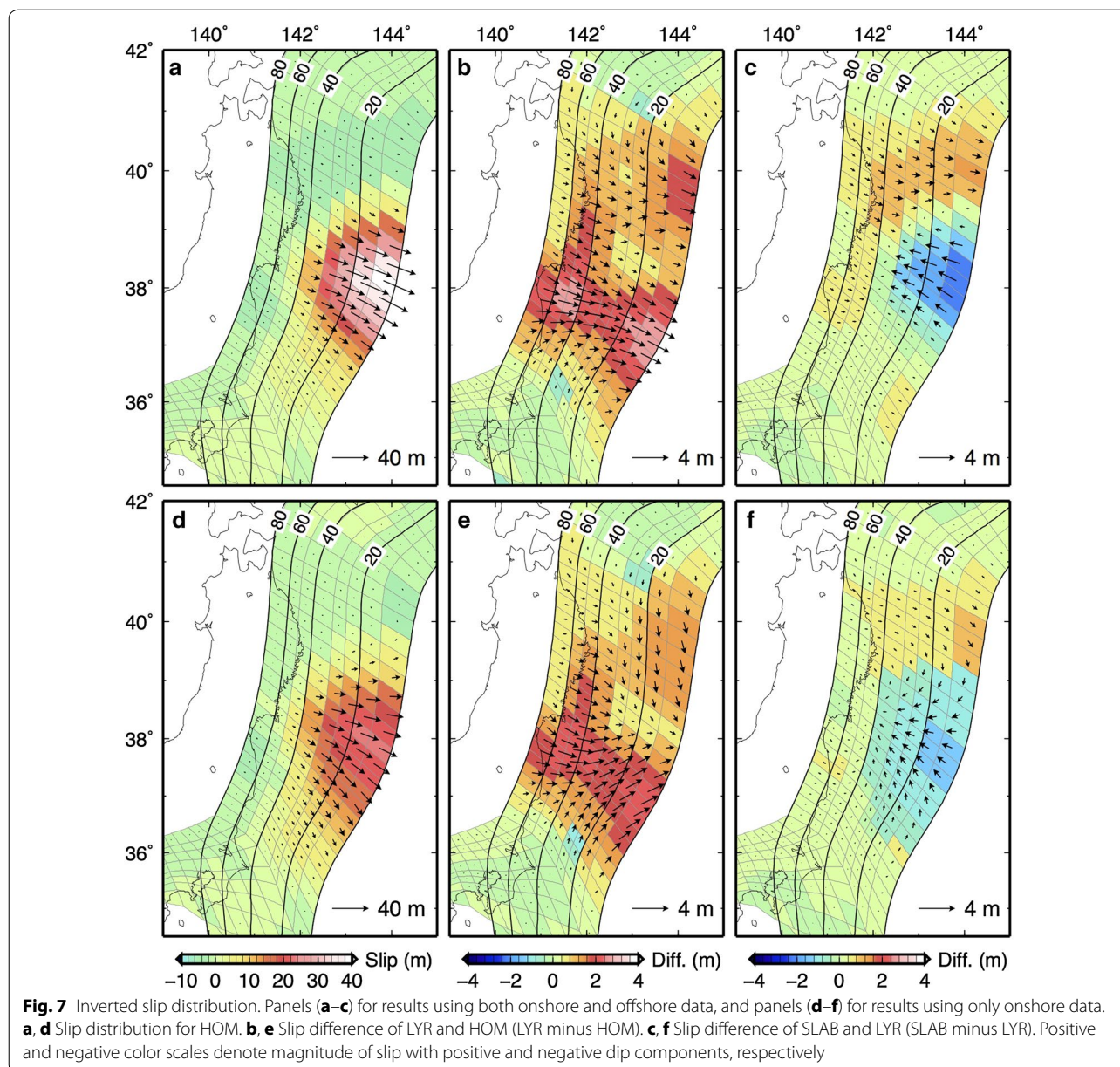
(SLAB), as expected from the background modulus increase. Seismic moment and potency in each structure are slightly smaller than those obtained in the combined inversion. These decreases are consistent with the findings of Diao et al. (2012) and Kyriakopoulos et al. (2013). Variance reduction generally indicates a better fit in each case compared to the corresponding combined inversion case. The offshore data are difficult to fit because they are biased by spatial sparseness, even for our weighting choices, and may include preseismic and postseismic deformation (Sato et al. 2011).

An interesting feature of these results is the increase and decrease in the maximum slip and potency from HOM to SLAB. We may understand these results by considering the layering and interface effects. In slip inversions, the layering effect requires larger slip given the increase in the average rigidity for the same surface displacements, and the interface effect requires smaller slip with the stronger footwall for the same surface displacements. A balance of these two effects controls the effect of the elastic structure on slip inversions. Comparing the layering and slab effects in slip inversions, the relative importance of the layering displacements is, naturally, larger for the purely layered case, and the relative importance of the interface displacements is larger in the slab case (Fig. 4). This would explain the increase in the maximum slip for LYR and their decrease compared to SLAB.

As we have seen, the offshore displacements are important for accounting for the effect of elastic structure close to the interface. One might expect that the maximum slip (and potency) would increase at LYR \rightarrow SLAB step without offshore data, because mainly the layering effect contributes. To the contrary, the result shows the maximum slip decreases for the combined inversion case. This contradiction can be understood by observing the vertical component. The vertical deformation can be more effective when we do not use the offshore data, because it is more localized in the closer (east) side of the land. From Fig. 4b, c, the change in the vertical displacement at HOM \rightarrow LYR and LYR \rightarrow SLAB steps is reversed in sign with the former characterized by decrease in subsidence (relative uplift), and the latter is characterized by the weak increase in subsidence (relative subsidence), though the relative subsidence area is placed more on north. Thus, to fit the data requires slip increase in LYR and slip decrease in SLAB. Given our results on the role of the Poisson's ratio, however, such subtle effects in the verticals may not be robust.

We examined three basic models to understand the basic behavior with changes in the overall elastic structure. Studies of seismic tomography, for example, indicate seismic velocity heterogeneity on smaller scales. We therefore further consider if an improvement in data fit can be achieved with possibly more realistic elastic structure. We take 1-D averaged vertical structure under Japan from seismic tomography (Matsubara et al. 2008) and elastic structure of the oceanic lithosphere from Miura et al. (2005). Mantle structure under the oceanic side is assumed to be the same as the continental sides. PAC and PHS slabs under the depth of 80 km are assumed to have 5 % larger seismic velocities than the surrounding mantle (Fig. 9a).

Figure 9 shows the inversion results. The overall slip distribution is similar to Figs. 6a and 7a. Compared



to SLAB, the maximum slip increases from 37.3 to 38.7 m and the potency increases from 1.16×10^{12} to $1.18 \times 10^{12} \text{ m}^3$. On the other hand, seismic moment decreases from 7.16×10^{22} to $5.61 \times 10^{22} \text{ Nm}$. These changes can be explained by the decrease in the interface effect due to the introduction of the weak oceanic crust. The residual pattern of data fit (Fig. 9c) is similar to SLAB, but the overall variance reduction reduced from 0.9981 to 0.9978. The slightly worse fit of the more “realistic” model may be due to a bias arising from the application of regional 3-D continental and oceanic velocity structures to our layered model structure and is likely not a comprehensive test of other 3-D heterogeneity.

However, this experiment serves to illustrate robustness of our results.

One might also be interested in effects of elastic structures on coseismic stress change. However, given our simplified elastic structures with little lateral heterogeneity, we find very little difference for shallow stress in terms of both amplitude and style of the stress tensor throughout the domain.

Discussion

We examined elastic effects on coseismic deformation due to the 2011 Tohoku-oki earthquake, Japan, with forward and inverse approaches. Several inversions using

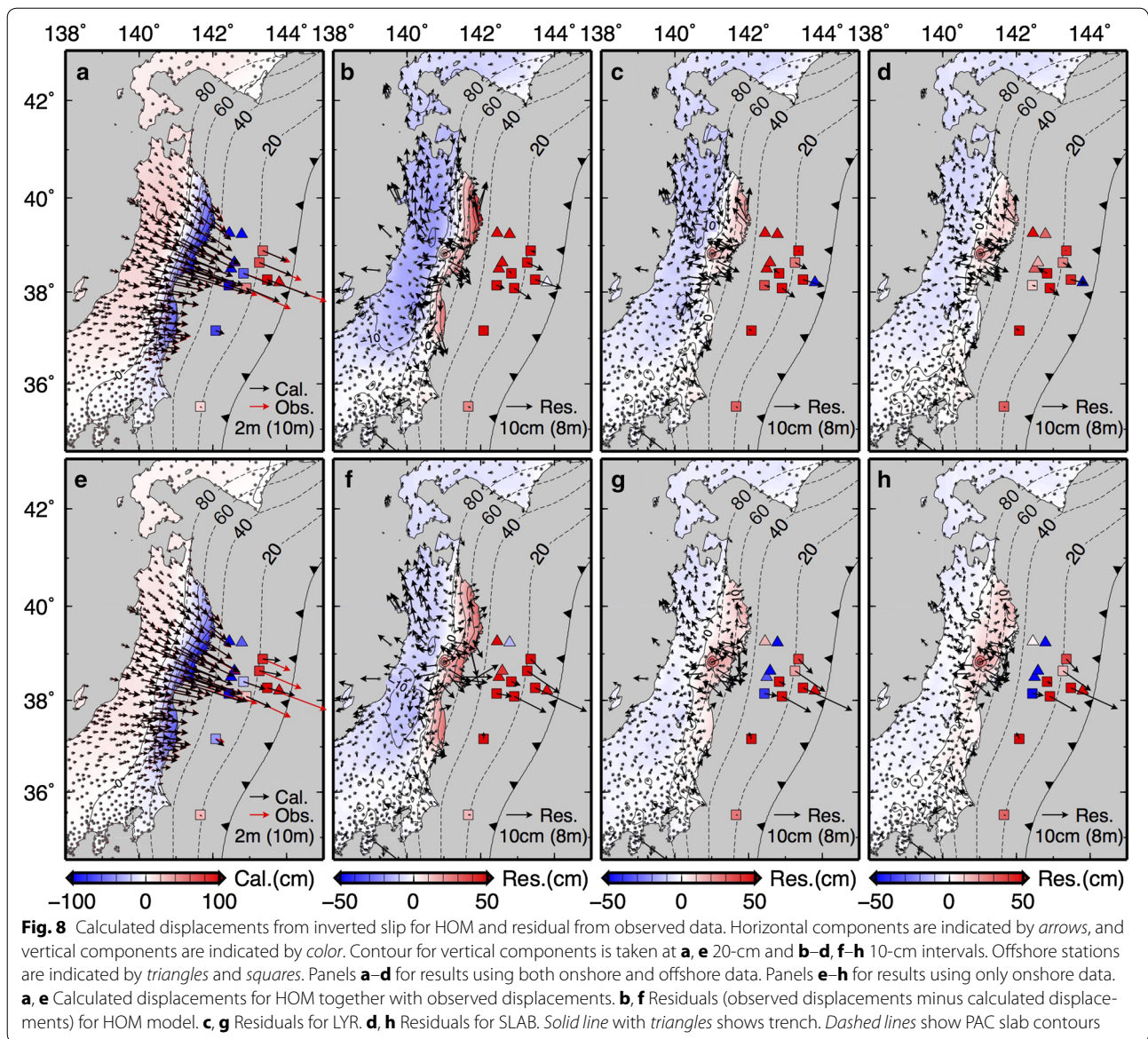
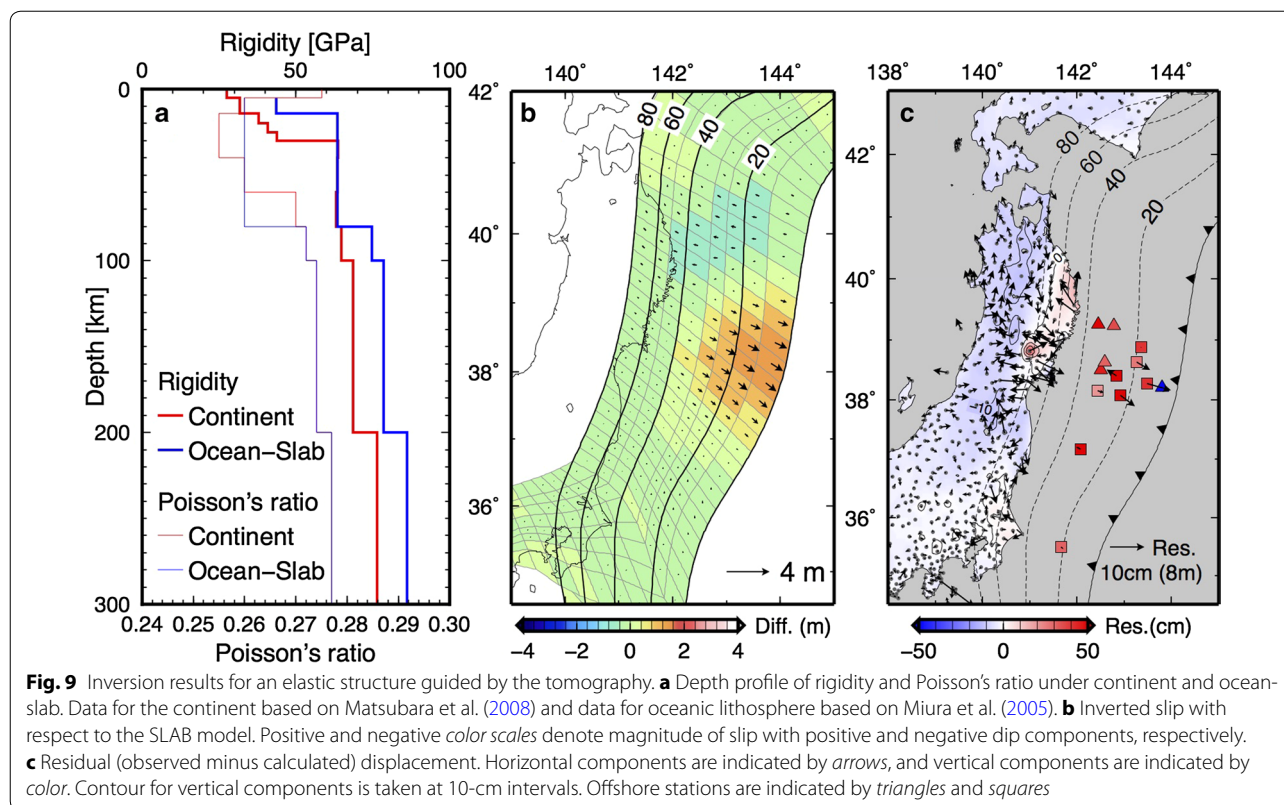


Table 1 Parameters for slip distribution and variance reduction (VR) in different elastic structures

| | HOM | LYR | SLAB | HOM* | LYR* | SLAB* |
|--------------------------------------|--------|--------|--------|--------|--------|--------|
| Maximum slip (m) | 38.5 | 39.6 | 37.3 | 22.4 | 23.2 | 22.0 |
| Potency (10^{12} m ³) | 1.06 | 1.18 | 1.16 | 0.95 | 1.00 | 0.97 |
| Moment (10^{22} Nm) | 3.72 | 4.49 | 7.16 | 3.31 | 4.01 | 6.07 |
| Magnitude | 8.98 | 9.04 | 9.17 | 8.95 | 9.00 | 9.12 |
| VR | 0.9956 | 0.9973 | 0.9981 | 0.9988 | 0.9993 | 0.9994 |
| VR (horizontal) | 0.9968 | 0.9979 | 0.9985 | 0.9992 | 0.9995 | 0.9995 |
| VR (vertical) | 0.4240 | 0.7290 | 0.7901 | 0.6262 | 0.8372 | 0.8620 |
| VR (onshore) | 0.9985 | 0.9991 | 0.9993 | 0.9988 | 0.9993 | 0.9994 |
| VR (offshore) | 0.9332 | 0.9588 | 0.9719 | – | – | – |

VR for horizontal and vertical components and for the onshore and offshore regions are also shown. Structure name without and with star indicates inversion results using both onshore and offshore data and using only onshore data, respectively



elastic heterogeneity have been published already. For the layering effects, our results are consistent with an increase in the seismic moment, but not consistent in terms of increasing the maximum slip (Pollitz et al. 2011; Diao et al. 2012; Dong et al. 2014). This is likely because we adopted a stronger smoothing constraint on the slip distribution, adjusting the damping based on consistent trade-off curve analysis. However, the bulk parameter seismic potency is a more robust measure to assess the elastic effect.

As for the slab effect, our results do not indicate a significant role of contrasts in rigidity across the plate interface compared to crust–mantle layering. Instead, fitting in the onshore region also plays an important role. This result conflicts with Kyriakopoulos et al. (2013), who emphasized its importance. One of the reasons for this mismatch might stem from the elastic contrast used. The rigidity ratio in our SLAB model is 2.4, while Kyriakopoulos et al.'s (2013) model used 3.7. According to studies of seismic tomography (e.g., Nakajima et al. 2001; Huang et al. 2011), velocity anomalies (V_p and V_s) in the slab compared to the surrounding mantle are $\sim 6\%$, implying that even our contrast might be on the high end. Kyriakopoulos et al.'s (2013) larger contrast may lead to an overestimate of the effect of elastic heterogeneity. Their elastic contrast also leads to poor fit of the vertical

displacements (Fig. 4c in Kyriakopoulos et al. 2013). Additionally, their choice of large Poisson's ratio of 0.34 for continental crust may also cause an underestimate of vertical displacements (Fig. 5h). Studies of seismic tomography do not support V_p/V_s ratios corresponding to such a high Poisson's ratio except in the toe part of the overriding plate (Matsubara and Obara 2011; Yamamoto et al. 2014).

We can understand the effects of elastic heterogeneity on inversions for subduction zone earthquake slip by considering layering and interface effects. While Earth's mantle shows lateral heterogeneity, the Moho and the plate interfaces are the most prominent discontinuities in the upper mantle. The inclusion of further heterogeneity for the example of Fig. 9 did not improve the fitting, though other model choices may of course perform better. Our results suggest that coseismic deformation cannot resolve elastic heterogeneity much beyond crust–mantle layering and the effects of a slab except for small-scale, lateral heterogeneities near the surface such as local topography. Slip distributions change from HOM \rightarrow LYR to LYR \rightarrow SLAB steps in different places (Fig. 7). This pattern cannot be explained by the overall layering and interface effects. It is likely due to the subtle geometry of plate boundary. If we would have a data set that stretches from the trench to land, a more

comprehensive understanding might be possible based on the two effects. Conversely, incompleteness of data, such as lack of the offshore data, may lead to difficulty in inferring the individual elastic effects.

In this study, the SLAB model shows the best data fit (Table 1). Still, we can see systematic residuals (Fig. 8d). Most notably, vertical residuals are positive on the east coast and negative in the west coast. This broad anomaly might reflect regional elastic heterogeneity, in particular of Poisson's ratio, with distance from the trench to the back-arc. Alternatively, the crustal thickness may gradually thin westward, or it could be attributed to the existence of an oceanic crust in the Sea of Japan and the thinned crust in the Miocene back-arc rift basin along the west coast (Matsubara et al. 2008). In this study, we did not consider lateral changes in crustal thickness, but such complexities would be straightforward to implement, and we expect that the misfit would be further reduced. We can also see a large positive vertical residual at (141°E, 39°N). This could be because of the local subsidence due to the hot material under a nearby volcano (Takada and Fukushima 2013), though the volcano itself is located slightly to the west.

Systematic horizontal residual vectors are also found in Fig. 8d. Westward-oriented residuals are found along the west coast and northward residuals on both sides of the strait at 41.5°N, which are also found in previous studies (Iinuma et al. 2012; Perfettini and Avouac 2014). The residuals along the west coast might be related to the thin oceanic crust of the Sea of Japan and the Miocene back-arc rift basin. The northward residuals around the strait might reflect some regional tectonics around the corner of the plate boundary zone between the northeast Japan and Kuril arcs. More strongly localized residuals on the east coast may be related to local elastic heterogeneities in the crust (Ohzono et al. 2012).

Conclusions

We investigated effects of elastic structure on coseismic deformation due to the 2011 Tohoku-oki earthquake, Japan, with a 3-D finite element model with forward and inverse approaches. We observed two main effects of heterogeneity for fixed slip tests: (1) On large spatial scales, elastic layering leads to a decrease in surface displacement with an increase in the average rigidity. (2) Close to the slab interface, surface displacements increase with the increase in rigidity across the fault. Both layered structure and slab effects are expressed as the superposition of the layering and interface effects. We also found that the vertical displacement modification due to slab structure was sensitive to the Poisson's ratio of the continental crust.

When the heterogeneous models are employed in inversions, the maximum slip increases from 38.5 m in the homogeneous to 39.6 m in the layered case and decreases to 37.3 m when slabs are introduced, and potency changes accordingly. While only of order 5–10 % of the maximum slip, patterns of local slip modification are robust, and the rheologically more realistic models do provide a better fit to the data. Inclusion of slip on the Philippine Sea plate interface has little impact. Further improvements of data fit may therefore be possible by introducing local heterogeneity near the surface and local topography.

Among the elastic heterogeneity effects, layering has the larger impact on inferred slip and leads to a broader and deeper slip patch compared to the homogeneous model, particularly to the south of the overall slip maximum. The further introduction of a strong slab leads to a reduction in slip around the maximum slip and a slight increase further toward the north, both effects localized close to the trench. While heterogeneity is thus of minor importance for bulk properties such as potency, a layered medium with a slab shows a systematically modified response, and the inferred differences in slip distribution may matter for detailed regional effects, such as inferences on afterslip or viscoelastic relaxation.

Abbreviations

PHS: Philippine Sea plate; EUR: Eurasian plate; PAC: Pacific plate; HOM: homogeneous structure; LYR: layered structure; SLAB: slab structure.

Authors' contributions

AH explored the elastic effects, performed the computations, and prepared the manuscript. TWB contributed to the inversion results, their interpretation, and study design. AH and AMF made the finite element model. HS provided the structural data for constructing the finite element model. AH and DAO made the model of plate boundaries. All authors read and approved the final manuscript.

Author details

¹ Earthquake Research Institute, University of Tokyo, Yayoi 1-1-1, Bunkyo-ku, Tokyo 113-0032, Japan. ² Department of Earth Sciences, University of Southern California, Los Angeles, CA, USA. ³ Present Address: Jackson School of Geosciences, The University of Texas at Austin, Austin, TX, USA. ⁴ Department of Earth, Atmospheric, and Planetary Sciences, Purdue University, West Lafayette, IN, USA.

Acknowledgements

We would like to thank Editor Azusa Nishizawa and two anonymous reviewers for their comments which improved our manuscript. We are grateful to Hisashi Suito, Yuki Hatanaka, and Hiroshi Yurai for providing the GPS data. We would like to thank the Hydrographic and Oceanographic Department of Japan Coast Guard for providing the offshore data. This study is supported by the Special Project for Reducing Vulnerability for Urban Mega Earthquake Disasters, the Integrated Research Project on Seismic and Tsunami hazards around the Sea of Japan, and the Earthquake and Volcano Hazards Observation and Research Program from the Ministry of Education, Culture, Sports, Science, and Technology of Japan (AH and HS), and the National Science Foundation under grant EAR-1215358 (AMF) and EAR-1215757 (TWB and DAO). Most figures were prepared with the use of the Generic Mapping Tools (Wessel and Smith, 1998).

Competing interests

The authors declare that they have no competing interests.

Appendix: Expression for the roughness matrix

The roughness matrix \mathbf{L} is constructed with the discretized Laplace operator for strike and dip slip components as described below. We may approximate the Laplace operator for slip element x_i at the center of patch i using distance to the surrounding patch centers r_{ik} in the form,

$$\nabla^2 x_i \approx \frac{m}{\bar{r}_i^2} \left(\frac{1}{C} \sum_{k=1}^n \frac{x_k}{(r_{ik})^2} - x_i \right), \quad (6)$$

where C is the normalizing constant, \bar{r}_i is the average distance to the surrounding patches, n is the number of the surrounding patches and m is the geometric constant. C and \bar{r}_i are written as

$$C = \sum_{k=1}^n \frac{1}{(r_{ik})^2}, \quad \bar{r}_i = \frac{1}{n} \sum_{k=1}^n r_{ik}. \quad (7)$$

n and m take the different values with respect to location in the source region: $n = 6$ and $m = 4$ for the patches inside, $n = 5$ and $m = 3$ for the patches on the edge, and $n = 3$ and $m = 2$ for the corner patches. Note that we use only 6 patches from 8 neighboring patches and likewise for edge patches, considering that the alignment of the patches is generally oblique and twisted. Then, explicit expression for L_{ij} is as follows,

$$L_{ij} = \frac{m}{\bar{r}_i^2} (j = i), \quad L_{ij} = \frac{m}{\bar{r}_i^2} \frac{1}{C(r_{ik})^2} \quad (\text{neighboring patch}), \quad L_{ij} = 0 \quad (\text{otherwise}). \quad (8)$$

Received: 3 June 2016 Accepted: 14 September 2016

Published online: 23 September 2016

References

- Ampuero J-P, Dahlen FA (2005) Ambiguity of the moment tensor. *Bull Seismol Soc Am* 95:390–400
- Baba T, Tanioka Y, Cummins PR, Uihira K (2002) The slip distribution of the 1946 Nankai earthquake estimated from tsunami inversion using a new plate model. *Phys Earth Planet Inter* 132:59–73
- Diao FQ, Xiong X, Zheng Y (2012) Static slip model of the Mw 9.0 Tohoku (Japan) earthquake: results from joint inversion of terrestrial GPS data and seafloor GPS/acoustic data. *Chin Sci Bull* 57:1990–1997
- Dong J, Sun W, Zhou X, Wang R (2014) Effects of Earth's layered structure, gravity and curvature on coseismic deformation. *Geophys J Int* 199:1442–1451. doi:10.1093/gji/ggu342
- Fujii Y, Satake K, Sakai S, Shinohara M, Kanazawa T (2011) Tsunami source of the 2011 off the Pacific coast of Tohoku Earthquake. *Earth Planets Space* 63:815–820
- Hayes GP, Wald DJ, Johnson RL (2012) Slab1.0: a three-dimensional model of global subduction zone geometries. *J Geophys Res* 117:B01302. doi:10.1029/2011JB008524
- Hearn E, Bürgmann R (2005) The effect of elastic layering on inversions of GPS data for coseismic slip and resulting stress changes: strike-slip earthquakes. *Bull Seismol Soc Am* 95:1637–1653
- Hino R, Ito Y, Suzuki K, Suzuki S, Inazu D, Linuma T, Ohta Y, Fujimoto H, Shinohara M, Kaneda Y (2011) Foreshocks and mainshock of the 2011 Tohoku Earthquake observed by ocean bottom seismic/geodetic monitoring. Abstract of AGU 2011 Fall Meeting U51B-0008
- Hirose F, Nakajima J, Hasegawa A (2008a) Three-dimensional seismic velocity structure and configuration of the Philippine Sea slab in southwestern Japan estimated by double-difference tomography. *J Geophys Res* 113:B09315. doi:10.1029/2007JB005274
- Hirose F, Nakajima J, Hasegawa A (2008b) Three-dimensional velocity structure and configuration of the Philippine Sea slab beneath Kanto district, central Japan, estimated by double-difference tomography (in Japanese with English abstract). *J Seismol Soc Jpn* 60:123–138
- Hsu Y-J, Simons M, Williams C, Casarotti E (2011) Three-dimensional FEM derived elastic Green's functions for the coseismic deformation of the 2005 Mw 8.7 Nias-Simeulue, Sumatra earthquake. *Geochem Geophys Geosyst* 12:Q07013. doi:10.1029/2011GC003553
- Huang Z, Zhao D, Wang L (2011) Seismic heterogeneity and anisotropy of the Honshu arc from the Japan Trench to the Japan Sea. *Geophys J Int* 184:1428–1444
- linuma T, Ohzono M, Ohta Y, Miura S (2011) Coseismic slip distribution of the 2011 off the Pacific coast of Tohoku Earthquake (M 9.0) estimated based on GPS data—Was the asperity in Miyagi-oki ruptured? *Earth Planets Space* 63:643–648
- linuma T, Hino R, Kido M, Inazu D, Osada Y, Ito Y, Ohzono M, Tsushima H, Suzuki S, Fujimoto H, Miura S (2012) Coseismic slip distribution of the 2011 off the Pacific Coast of Tohoku Earthquake (M9.0) refined by means of seafloor geodetic data. *J Geophys Res* 117:B07409. doi:10.1029/2012JB009186
- Ishibe T, Shimazaki K, Satake K, Tsuruoka H (2011) Change in seismicity beneath the Tokyo metropolitan area due to the 2011 off the Pacific coast of Tohoku Earthquake. *Earth Planets Space* 63:731–735
- Ito Y, Tsuji T, Osada Y, Kido M, Inazu D, Hayashi Y, Tsushima H, Hino R, Fujimoto H (2011) Frontal wedge deformation near the source region of the 2011 Tohoku-Oki earthquake. *Geophys Res Lett* 38:L00G05. doi:10.1029/2011GL048355
- Kido M, Osada Y, Fujimoto H, Hino R, Ito Y (2011) Trench-normal variation in observed seafloor displacements associated with the 2011 Tohoku-Oki earthquake. *Geophys Res Lett* 38:L24303. doi:10.1029/2011GL050057
- Kita S, Okada T, Hasegawa A, Nakajima J, Matsuzawa T (2010) Anomalous deepening of a seismic belt in the upper-plane of the double seismic zone in the Pacific slab beneath the Hokkaido corner: possible evidence for thermal shielding caused by subducted forearc crust materials. *Earth Planet Sci Lett* 290:415–426
- Kyriakopoulos C, Masterlark T, Stramondo S, Chini M, Bignami C (2013) Coseismic slip distribution for the Mw 9 2011 Tohoku-Oki earthquake derived from 3-D FE modeling. *J Geophys Res* 118:3837–3847
- Maeda T, Furumura T, Sakai S, Shinohara S (2011) Significant tsunami observed at ocean-bottom pressure gauges during the 2011 off the Pacific coast of Tohoku Earthquake. *Earth Planets Space* 63:803–808
- Matsubara M, Obara K (2011) The 2011 off the Pacific coast of Tohoku Earthquake related to a strong velocity gradient with the Pacific plate. *Earth Planets Space* 63:663–667
- Matsubara M, Obara K, Kasahara K (2008) Three-dimensional P- and S-wave velocity structures beneath the Japan Islands obtained by high-density seismic stations by seismic tomography. *Tectonophysics* 454:86–103
- Menke W (2012) *Geophysical data analysis: discrete inverse theory, MATLAB edn (3rd edn)*. Academic Press (Elsevier), Waltham
- Miura S, Takahashi N, Nakanishi A, Tsuru T, Kodaira S, Kaneda Y (2005) Structural characteristics off Miyagi forearc region, the Japan Trench seismogenic zone, deduced from a wide-angle reflection and refraction study. *Tectonophysics* 407:165–188
- Nakajima J, Hasegawa A (2006) Anomalous low-velocity zone and linear alignment of seismicity along it in the subducted Pacific slab beneath Kanto, Japan: reactivation of subducted fracture zone? *Geophys Res Lett* 33:L16309. doi:10.1029/2006GL026773
- Nakajima J, Hasegawa A (2007) Subduction of the Philippine Sea plate beneath southwestern Japan: slab geometry and its relationship to arc magmatism. *J Geophys Res* 112:B08306. doi:10.1029/2006JB004770

- Nakajima J, Matsuzawa T, Hasegawa A, Zhao D (2001) Three-dimensional structure of V_p , V_s , and V_p/V_s beneath northeastern Japan: implications for arc magmatism and fluids. *J Geophys Res* 106:21843–21857
- Nakajima J, Hirose F, Hasegawa A (2009) Seismotectonics beneath the Tokyo metropolitan area, Japan: effect of slab-slab contact and overlap on seismicity. *J Geophys Res* 114:B08309. doi:10.1029/2008JB006101
- Nishimura T, Munekane H, Yurai H (2011) The 2011 off the Pacific coast of Tohoku Earthquake and its aftershocks observed by GEONET. *Earth Planets Space* 63:631–636
- Ohzono M, Yabe Y, Iinuma T, Ohta Y, Miura S, Tachibana K, Sato T, Demachi T (2012) Strain anomalies induced by the 2011 Tohoku Earthquake (Mw 9.0) as observed by a dense GPS network in northeastern Japan. *Earth Planets Space* 64:1231–1238
- Ozawa S, Nishimura T, Suito H, Kobayashi T, Tobita M, Imakiire T (2011) Coseismic and postseismic slip of the 2011 magnitude-9 Tohoku-Oki earthquake. *Nature* 475:373–376
- Ozawa S, Nishimura T, Munekane H, Suito H, Kobayashi T, Tobita M, Imakiire T (2012) Preceding, coseismic, and postseismic slips of the 2011 Tohoku earthquake, Japan. *J Geophys Res* 117:B07404. doi:10.1029/2011JB009120
- Perfettini H, Avouac JP (2014) The seismic cycle in the area of the 2011 Mw9.0 Tohoku-Oki earthquake. *J Geophys Res* 119:4469–4515. doi:10.1002/2013JB010697
- Pollitz FF, Bürgmann R, Banerjee P (2011) Geodetic slip model of the 2011 Mw9.0 Tohoku earthquake. *Geophys Res Lett* 38:L00G08. doi:10.1029/2011GL048632
- Pulvirenti F, Jin S, Aloisi M (2014) An adjoint-based FEM optimization of coseismic displacements following the 2011 Tohoku earthquake: new insights for the limits of the upper plate rebound. *Phys Earth Planet Inter* 237:25–39
- Romano F, Trasatti E, Lorito S, Piromallo C, Piatanesi A, Ito Y, Zhao D, Hirata K, Lanucara P, Cocco M (2014) Structural control on the Tohoku earthquake rupture process investigated by 3D FEM, tsunami and geodetic data. *Sci Rep* 4:5631. doi:10.1038/srep05631
- Sagiya T, Miyazaki S, Tada T (2000) Continuous GPS array and present-day crustal deformation of Japan. *Pure appl Geophys* 157:2303–2322
- Sato M, Ishikawa T, Ujihara N, Yoshida S, Fujita M, Mochizuki M, Asada A (2011) Displacement above the hypocenter of the 2011 Tohoku-oki earthquake. *Science* 332:1395
- Smith WHF, Wessel P (1990) Gridding with continuous curvature splines in tension. *Geophysics* 55:293–305
- Suzuki W, Aoi S, Sekiguchi H, Kunugi T (2011) Rupture process of the 2011 Tohoku-Oki mega-thrust earthquake (M9.0) inverted from strong motion data. *Geophys Res Lett* 38:L00G16. doi:10.1029/2011GL049136
- Takada Y, Fukushima Y (2013) Volcanic subsidence triggered by the 2011 Tohoku earthquake in Japan. *Nature Geosci* 6:637–641
- Wessel P, Smith WHF (1998) New, improved version of the generic mapping tools released. *EOS Trans AGU* 79:579
- Yagi Y, Fukahata Y (2011) Rupture process of the 2011 Tohoku-oki earthquake and absolute elastic strain release. *Geophys Res Lett* 38:L19307. doi:10.1029/2011GL048701
- Yamamoto Y, Obana K, Kodaira S, Hino R, Shinohara M (2014) Structural heterogeneities around the megathrust zone of the 2011 Tohoku earthquake from tomographic inversion of onshore and offshore seismic observations. *J Geophys Res* 119:1165–1180

Submit your manuscript to a SpringerOpen® journal and benefit from:

- Convenient online submission
- Rigorous peer review
- Immediate publication on acceptance
- Open access: articles freely available online
- High visibility within the field
- Retaining the copyright to your article

Submit your next manuscript at ► springeropen.com
